A 10 tesla table-top controlled waveform magnet

Aditya N. Roy Choudhury[a] and V. Venkataraman
Department of Physics, Indian Institute of Science, Bangalore 560012, India

(Received 16 February 2012; accepted 15 March 2012; published online 4 April 2012)

Controlled waveform magnets (CWMs) are a class of pulsed magnets whose pulse shape with time can be programmed by the user. With a CWM, the user gains control not only over the magnitude of the field but also over its rate of change. In this work we present a table-top CWM, driven by a capacitor bank, capable of producing virtually any user-shaped magnetic field waveform up to 10 tesla. Insulated gate bipolar transistor chips have been paralleled to form the high current switch and paralleled chips of SiC Schottky diodes form the crowbar diode module. Sample controlled waveforms including flat-tops up to 10 tesla and some triangular magnetic field pulses have been successfully generated for 10–20 ms with a ripple <1%. © *2012 American Institute of Physics*. [http://dx.doi.org/10.1063/1.3699316]

I. INTRODUCTION

A. Controlled waveform magnets

High magnetic fields are indispensable for modern-day solid state research and pulsed magnets have been an essential part of it.[1,2] Whereas commonly available dc electromagnets can produce fields up to ∼1 tesla and standard superconducting magnets up to 12–15 tesla, a pulsed magnet – energized by hundreds of kilojoules of energy from a standard capacitor bank – can produce fields of the order of 50 tesla.[1] Controlled waveform magnets (CWMs) (Refs. 1 and 3–5) are a class of magnets whose field-vs.-time profile can be shaped at will. The inception of such a magnet came from the motivation of studying metallic samples[6] or thermal responses[7] at high magnetic fields for which the field needed to be steady for a minimum period of time (for 100 s of milliseconds, even up to 1 or 2 s). CWMs have also been used for high field magneto-resistance measurements[8] and high field magnetization measurements[9–12] with magnetic field ramps (fields varying linearly with time) and step-wise magnetic field pulses.

B. Application of controlled magnetic field waveforms

Controlling the waveform allows one to produce stable (our table-top setup gives a ripple <1%) and quasi-stationary (pulse widths up to 100 s of ms in big CWM installations, and up to 10 s of ms in our table-top setup), high magnetic fields among a variety of other possible pulse shapes. References 3, 13, and 14 give an overview of the research that was carried out in the Amsterdam and the Los Alamos NHMFL CWM facilities a decade back. Interesting work on the effects of trapezoidal magnetic field waveforms on metals and type II superconductors are discussed in Refs. 15 and 16. Some measurements on high temperature superconductors[17] directly reveal the dependence of the measured magnetization on the field-sweep-rate. Pulsed fields can be used to magnetize various materials of which the work concerning the magnetization of high temperature superconductors with the "WCPM technique"[18,19] deserves special mention.

C. Various pulse shaping techniques

Literature cites three major ways of temporally controlling the magnetic field waveform. Approximate flat-tops can be produced in a pulsed magnet by making the field exponentially decay through a crowbar diode with a very large time-constant (large L/R) once the field has reached its peak. The end of the flat-top occurs at a point where the current path is suddenly switched to a different crowbar path that has a faster decay, which is usually done to minimize magnet coil heating. Examples of such work are given in Refs. 20 and 21 where the idea is implemented to produce fields <1 tesla, although extending it to a higher field regime is very possible. The prime disadvantage of this method is that it is approximate and hardly any shapes other than the flat-top can be produced. Pulse forming networks (PFNs) (Ref. 22) provide another way in which current pulses can be shaped with time where individual LC circuit currents can be added up through a Fourier series to provide any user-desired pulse shape. Here, the primary disadvantages are that too many components make the setup bulky and the pulse shape with time cannot be changed for a given PFN. The advantage, however, is that complex pulse shapes can be achieved and the resulting controlled waveform is free from noise. The third method is feedback regulation of the voltage applied to a magnet coil – thus controlling the magnet current with time (virtually all CWM facilities worldwide operate with this principle[1]), or regulation of the magnet current directly through feedback as described in Refs. 23 and 24, or in our work. This method can effectively produce any controlled field waveform, although, an inherent high frequency ripple accompanies the regulation of the magnet current. However, we have been able to achieve a ripple <1%.

D. Absence of a CWM as table-top lab equipment

Pulse shaping (mostly flat-tops) is widely practiced in magnets used for plasma physics research[25] where they are mostly used to shape the fields of the synchrotrons' injection/extraction kicker magnets. However, the fields associated there are <1 tesla. In summary, literature provides ample

[a]Electronic mail: aditya@physics.iisc.ernet.in.

instances for shaped magnetic fields and pulse shaping methods at fields <1 tesla (where the magnetic field is not sufficiently large to be used as an experimental probe in solid state physics) and >25 tesla (where it is rather a national facility and not a laboratory equipment that can be used on a day-to-day basis). This leaves a vacuum in the pulse shaping practices in the 1–25 tesla field regime.

II. SETUP

A. The table-top CWM and its operating principle

A table-top capacitor bank, made by paralleling 13 individual electrolytic capacitors – 4.7 mF/ 450 V each – forms the power supply. It is connected in series with a magnet coil and a high current switch. Insulated gate bipolar transistors (IGBTs) are chosen as the high current switch. The bank can be charged (to some "charging voltage" $V_0 < 450$ V) and then discharged into the magnet through the IGBTs. The magnet current is pulse modulated by switching the IGBTs on and off with a gate signal. The gate signal is isolated from the high current circuitry. A crowbar diode module is connected anti-parallel across the inductive load for freewheeling of the magnet current when the switch turns off.

Here, we have paralleled 20 individual IGBT chips from International Rectifier: IRG4PH50U, although a commercially available IGBT module is also a feasible option as long as it can carry high currents (≥1 kA) and can switch fast enough to allow a small field ripple. Since we also wanted to conjecture that our setup can be scaled up to still higher magnetic fields, we demonstrate IGBT paralleling here with individual high frequency IGBT chips. Paralleling also helps us to put individual snubbers placed very close to each IGBT chip thus minimizing the snubber path inductances.

A closed-loop Hall-effect based current transducer from LEM: LF 2005-S, with a frequency bandwidth of 100 kHz (–1 dB) and a maximum sensing capacity of 2 kA, measures the time-varying magnet current precisely and converts it to a proportionate voltage; the current-to-voltage scaling factor can be set externally by the secondary current load resistor R_{CT}. This voltage is fed to the negative input pin of a comparator LM311, which accounts for the negative feedback we have used in our design. The positive input pin of the comparator carries the "user-reference" – a voltage pulse fed through a standard function generator: Tektronix AFG3021B – which the magnetic field is supposed to "follow." R_{CT} determines the current-to-voltage conversion and the magnet coil determines the current-to-field conversion (B/I). The comparator output is connected to the gate of the IGBT, through the Semikron IGBT Driver – SKHI 10/17 which is able to source/sink output currents up to 8 A. A schematic diagram of the setup follows in Fig. 1.

B. Choosing the IGBT and the crowbar diode

IGBTs are chosen, over other current switches such as Power metal oxide semiconductor field effect transistors (MOSFETs), owing to their lower power dissipation while carrying high currents. Being bipolar in nature, IGBTs exhibit

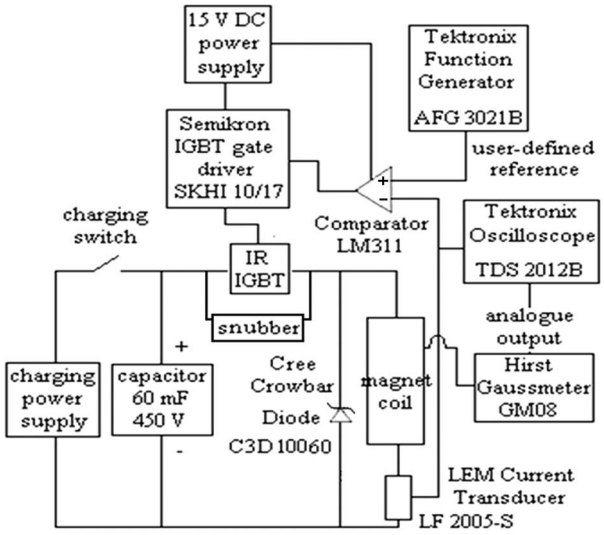

FIG. 1. Schematic of the table-top CWM.

lesser on-state losses owing to the phenomenon of conductivity modulation in their N-base and are thus preferred to MOSFETs for high power switching applications.[26] We initially checked our setup with various IGBTs, including modules, such as IRGPS40B120UD and IRG7PSH73K10PbF from International Rectifier, CM1000HA-24H from Mitsubishi and SKM800GA126D from Semikron. Once it was decided to parallel IGBTs, an obvious choice was chips rather than modules owing to a module's bigger size that may lead to significant spurious inductances and asymmetry in the collector path layout during paralleling. IRG4PH50U was finally chosen among various other chips owing to the maximum relative difference between its steady current (45–50 A) and pulsed current (180 A) ratings, its cost-effectiveness and easy availability in large numbers (required for sorting devices before paralleling), its maximum switching frequency around 40 kHz, and the availability of a SPICE model.

A PN junction diode (Semikron SKR 320/16) was initially used as the crowbar diode but it was later found that reverse recovery current spikes originating from it during the fast switching were causing the IGBTs to break down, mostly at high charging voltages ($V_0 > 250$ V). The recent advent of the "zero-recovery" high voltage SiC Schottky diode solves this problem. Twenty individual chips of 10A/600V SiC Schottky diodes from CREE: C3D10060 were paralleled to form the crowbar diode module. This was seen to carry a pulsed load of 1 kA successfully. Our setup works better with the Schottky crowbar diodes, reducing the switching stresses on the IGBTs significantly as verified through SPICE simulations. Discussions on freewheeling diode reverse-recovery failure modes in IGBTs and clamped inductive switching dynamics in IGBTs exist in literature.[27,28] They shed light on how the phenomenon of reverse recovery or finite transit time in diodes can subject the high current switch to severe switching stresses, often leading to its breakdown.

C. Choosing a snubber for the IGBT

Non-idealities like the reverse recovery of the crowbar diode and the spurious inductance in the IGBT collector

current paths make the use of snubbers necessary. Reference 29 gives a nice overview of the type of snubbers that should be used for IGBT applications. Capacitors added externally across the IGBTs help to keep the transient collector-emitter voltages (V_{CE}) within the safe operating area. However, snubber capacitors alone can cause additional current spikes. A finite resistance is needed in the snubber path, but using too high a resistance brings back the voltage spikes. To solve this optimization problem, we used resistor capacitor diode (RCD) snubbers.[30] The charging of the snubber capacitor takes place through a snubber diode and it is discharged rather slowly through a kΩ resistor placed parallel to the snubber diode.

We use one RCD snubber per IGBT. Electrolytic capacitors of 100 uF/450 V were used along with SiC Schottky diodes as the snubber network. Discharge resistors of value 10 kΩ/ 5 W were used, but they would not be required for a single pulse application. Yet we use them to prevent the snubber capacitors from getting over-charged if the CWM is operated repeatedly. The Schottky diode bypasses the resistor during charging and prevents voltage spikes, although it also adds a small amount of parasitic inductance. However, we have experimentally not observed significant IGBT collector-emitter voltage (V_{CE}) transients beyond the charging voltage V_0 (i.e., $V_{spike} < 100$ V). Note that in applications such as ours, IGBTs can undergo unpredictable breakdown if proper crowbar and snubbers are not used.

D. IGBT power dissipation

Heat dissipation in a switching device arises from its switching and conduction losses. This is dependent on the collector-emitter voltage (V_{CE}) and the collector current (I_C) of the IGBT. In our application, the IGBTs automatically adjust their switch-on and switch-off times (pulse width modulation through negative feedback) to control the magnet current. Hence, sometimes the IGBTs switch very fast and at other times rather slowly – giving rise to non-uniform power dissipation over time. To study this, the I_C waveforms can be recorded by using another current transducer in the concerned IGBT's collector current path. Similarly, V_{CE} can be sensed with a "10×" oscilloscope probe. The non-uniform power dissipation $P(t) = [V_{CE}(t) \times I_C(t)]$ can be numerically integrated to obtain the total energy dissipated in that pulse. This energy divided by the pulse width Δt will provide the mean power dissipation $P(\Delta t)$. Power dissipation will evidently increase as the magnet current or the capacitor bank charging voltage increases. The power dissipation can also be estimated from SPICE simulations.

The (junction-to-case) transient thermal impedance curve given in the IGBT datasheet is used to estimate the maximum power dissipation P_{limit} (Δt) that the device will be able to handle for a given pulse width Δt. Note that the maximum allowed power dissipation for an IGBT operating in a pulsed application such as ours can be higher than its steady-state power dissipation limit P_{limit} ($\Delta t \rightarrow \infty$) stated in the datasheet – which is a bonus. The steady-state junction-to-case transient thermal impedance $Z_{\theta JC}$ ($\Delta t \rightarrow \infty$) = 0.64 °C/W for an IRG4PH50U chip, but this value reduces to $Z_{\theta JC}$ (10 ms) ∼ 0.25 °C/W, or $Z_{\theta JC}$ (20 ms) ∼ 0.3 °C/W for shorter pulse widths. Considering 150 °C to be the junction temperature limit ($T_{J\text{-}limit}$) for safe operation of the IGBT and 25 °C (T_{case}) to be the room temperature, one arrives at: $T_{J\text{-}limit} = [T_{case} + P_{limit}(\Delta t) \times Z\theta_{JC}(\Delta t)] \Rightarrow P_{limit}$ (10 ms) ∼ 500 W and P_{limit} (20 ms) ∼ 415 W – values that are more than P_{limit} (∞) ∼ 195 W.

As the on-state voltage drop ($V_{CE\text{-}on}$) increases with higher currents handled, it is advisable not to drive each IGBT beyond its steady state current rating I_0 (for IRGPH50U, I_0 ∼ 50A) as that would end up increasing the conduction losses.

E. Electromagnetic interference (EMI) shielding and noise filtering

A small negative voltage can be added to the (+)ve input pin of the comparator chip to make sure that, while the capacitor bank is charging up, the background noise does not accidentally trigger the comparator (and thus the IGBTs). We added ∼−1.5 V externally, and the function generator output was accordingly adjusted.

Even with all protections against IGBT failure considered until now, the chips at times were observed to undergo unpredictable breakdown at high charging voltages ($V_0 > 250$ V). The reason was eventually tracked down to the capacitively coupled noise induced on the (+)ve input pin of the comparator leading the IGBT to switch randomly and dissipating more power than it can handle. IGBT gate-emitter voltage (V_{GE}) waveforms tested also verify this fact by showing the induced noise trying to spuriously turn the IGBT on or off. The source of this noise was verified to be the neighboring pin of the comparator that is carrying the current transducer output. The problem was solved by effectively filtering (passive 1st order RC filtering) the current transducer output. The comparator assembly was also electrically shielded from the other parts of the circuit in a grounded aluminum box – thus minimizing EMI. The co-axial cable connecting the function generator output and the comparator input, through BNC connectors, was minimized to <10 cm in length.

A filter cutoff (f_C) of 100 kHz substantially rules out the background noise problem and produces good results; this also does not affect the true current transducer output (–1 dB at 100 kHz). However, if f_C is decreased to lower frequencies, the output of the current transducer starts getting filtered out and thus, through feedback, affects the magnet current itself. Therefore, with a lower f_C, the IGBTs switch lesser number of times with reduced switching losses but evidently increasing the magnet current ripple. SPICE simulations can be an excellent guide to this optimization. Figure 2 shows the comparator circuit schematic.

Yet another method to improve the noise immunity of the setup and to actively control the trade-off between IGBT power dissipation and field ripple is to implement a Schmitt trigger with the comparator. This technique is so effective that the comparator circuit can be operated from a bread-board without requiring any EMI-shielding. However, the resulting ripple (∼10%) is unacceptable.

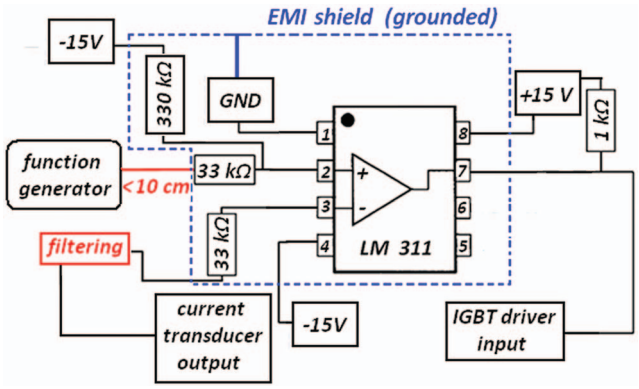

FIG. 2. Comparator LM311 block diagram showing the circuit connections.

F. Paralleling of IGBT and crowbar diode chips

Before paralleling, we tested a set of one IGBT chip, one RCD snubber (soldered very close to the IGBT leads), and one SiC Schottky crowbar diode with 50 A and 10 ms long controlled pulses up to a charging voltage of $V_0 = 350$ V and no IGBT breakdown was observed. Subsequent paralleling allowed us to increase the user-reference, without increasing V_0 further, thus increasing the magnetic field. V_{CE} transients were checked to be within limits. V_{GE} waveforms were also verified for absence of spurious IGBT turn on or off signals even in moderately noisy environments.

Guidelines for paralleling were followed from Ref. 31. Double-sided printed circuit boards (PCBs) were used instead of bus bars owing to the ready availability of PCBs and also because the PCB tracks can carry high transient currents without burning out. A 4 mm wide and 100 μm thick copper trace was provided for each chip and was observed to carry pulsed currents up to 100 A successfully. These tracks radiate out from a central contact, making the individual IGBT current paths equal in length and symmetric. A similar design follows on the bottom side of the PCB, effectively stacking the individual collector and emitter paths across the PCB thickness to minimize parasitic inductance.

Individual gate resistors of 22 Ω were added for each IGBT and extra care was taken to minimize and match the lengths of the wires that run from the gate and emitter of each chip to the driver output. "$V_{CE\text{-}on}$ screening"[31] of IGBT chips was performed before selecting devices for paralleling. Even in the same batch, IGBT chips were found to have a good amount of variation in their collector emitter on-state voltage drops (maximum $V_{CE\text{-}on}$ deviation among 25 random IGBT chips tested was found to be ~2 V)! After sorting, IGBTs were chosen such that the maximum deviation in the 20 $V_{CE\text{-}on}$ values is ~500 mV. Similar PCB design was used for constructing the crowbar diode module using Schottky diodes whose on-state voltage drop (V_{diode}) was matched as well. Maximum deviation that was allowed in V_{diode} was ~100 mV. Placing the IGBTs on a common heat sink is known to be another important paralleling criterion. However, we do not pursue that idea here essentially because ours is a pulsed project; heat takes some finite time to flow from the junction to the case and by that time the pulse is mostly over.

TABLE I. Magnet coil parameters.

Parameters	Coil 1	Coil 2
Winding wire	SWG 17	SWG 21
Bore size ($2a_1$)	1.2 cm	1.2 cm
Coil length (2b), α, β	6 cm, 2.8, 5	2.2 cm, 3, 1.8
F(α, β), No. of turns	2.3, 200	1.7, 364
Inductance	200 μH	2.06 mH
Resistance @ RT, @ LN2	171 mΩ, 27 mΩ	1.16 Ω, 177 mΩ
Peak field @ RT, @ LN2	9 tesla, 20 tesla	4.2 tesla, 15 tesla
(Central) Field : Current ratio (B/I)	0.0044 T/A	0.0147 T/A

Note that here we drive 20 paralleled IGBT chips with one Semikron driver SKHI 10/17. If more IGBTs or bigger IGBT modules need to be paralleled,[32] for scaling up our CWM to even higher fields, one would need more such IGBT drivers operating in parallel as well.

G. Magnet coils

Two magnet coils were used in our setup, viz., Coil 1 and Coil 2. Both were wound with ordinary copper wire. Coil 1 is used for room temperature (RT) controlled waveform generation and Coil 2 is meant for Liquid Nitrogen (LN2) temperature use. The magnet coil parameters are given in Table I. All inductances and resistances were measured with a HIOKI LCR meter – 3532-50. At LN2 the resistances of our magnets were seen to decrease from its room temperature value by ~6.5 times, although literature cites it can fall by as much as 8 times.[2] Magnetic field was measured by a hand-held gaussmeter (up to 3 tesla) and by a calibrated pick-up coil (beyond 3 tesla).

III. RESULTS AND DISCUSSIONS

A. Table-top CWM waveforms

Sample controlled waveforms from the table-top CWM follow in Figs. 3 and 4. Some flat-tops and triangular pulses are shown at room temperature and LN2 with Coil 1 and Coil

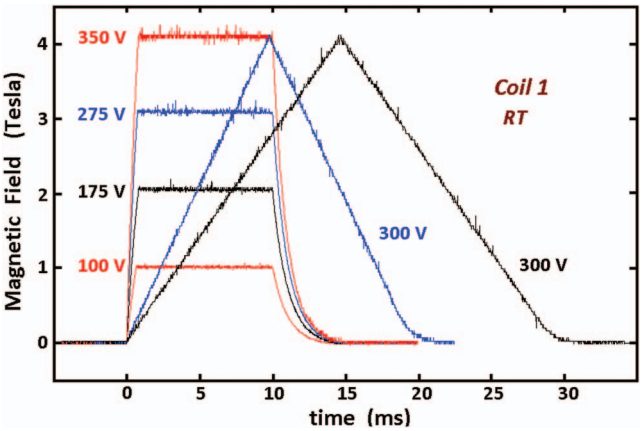

FIG. 3. Sample flat-tops and ramps with Coil 1 at room temperature (RT); numbers show charging voltage V_0 of the capacitor bank (in volts) used to generate these pulses. User-reference pulse fed is: 10 ms long for flat-tops, and 20 ms and 30 ms long for ramps, respectively. Ripple is <1%.

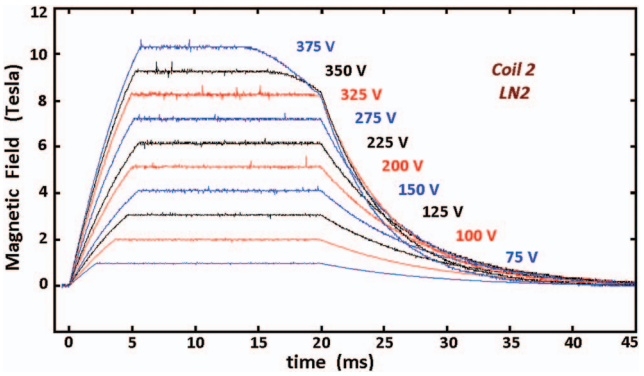

FIG. 4. Sample flat-tops with Coil 2 at liquid nitrogen temperature (LN2); numbers show charging voltage V_0 of the capacitor bank (in volts) used to generate these pulses. User-reference pulse fed is: 20 ms long. Ripple is <1%.

2, respectively. With our capacitor bank and magnet coils, and with a controlled pulse width in the order of 10 ms, we managed to reach up to 4 tesla at room temperature and up to 10 tesla at LN2.

Waveforms recorded are the current transducer outputs captured by the Tektronix oscilloscope TDS 2012B, accordingly scaled to magnetic field using the calibration constants R_{CT} and (B/I). The switching noise present in the above waveforms can be averaged out if several measurements are taken one after the other. This is illustrated in Fig. 5. Note that the field-sweep-rate in our table-top CWM can easily reach 100 s of tesla/s.

B. Controlled waveform ripple

Setting a low-pass filter with cutoff $f_C = 100$ kHz at the current transducer output, the background noise induced on the (+)ve input pin of the comparator chip can be significantly reduced. We tested our setup by using $f_C \sim 70$ kHz in one case and $f_C \sim 7$ kHz in another. The ripple obtained in the second case was observed to be at least 5 times higher compared to that in the first.

We have finally managed to bring down the ripple to acceptable values (<1%) [see Fig. 5(b)]. This is primarily due to the high switching frequency of the IGBTs. Simulations show that without noise and low-pass filtering, each IGBT chip would have dissipated almost 3 times the power that it dissipates with a filter of $f_C = 100$ kHz.

Ripple increases with charging voltage V_0 as rate of change of magnet current through the coil increases with charging voltage. This explains why we mostly see the magnitude of the ripple slowly decreasing along the width of the controlled pulse – because the voltage across the capacitor bank keeps decreasing. This phenomenon does not occur if a Schmitt trigger is used instead of a low pass filter – the ripple stays constant throughout the pulse width.

The ripple can yet be minimized by another independent technique – by designing[2] a magnet coil with high rise and fall times. However, with such coils, the variety of controlled waveforms that can be generated is limited. This is one of the reasons why we fail to show any reasonable controlled triangular pulses in Coil 2 since the magnetic field decays so slowly that it cannot follow a fast ramp-down of the user-reference.

Finally, the magnetic field ripple can also be reduced by putting a "short circuit ring" within the bore of the magnet as has been discussed in Ref. 5. However, this method is also known to reduce some of the accessible sample space inside the magnet bore.

C. Tailoring the controlled pulse width

The maximum duration that the magnet current can follow the reference pulse depends on the stored electrical energy. Simulations can be effectively used to estimate this duration for a certain user-defined pulse shape once the capacitor bank's charging voltage is fixed. In principle, standard calculations can be done based on charge conservation: input charge = product of capacitance and charging voltage, output charge = integrated area under the current-vs.-time waveform (after excluding the areas where the current is decreasing since that corresponds to freewheeling through the crowbar diode, during which time the capacitor bank remains disconnected from the magnet). Longer pulse widths at lower magnetic fields can be obtained with the same charging voltage; longer pulse widths with higher charging voltages

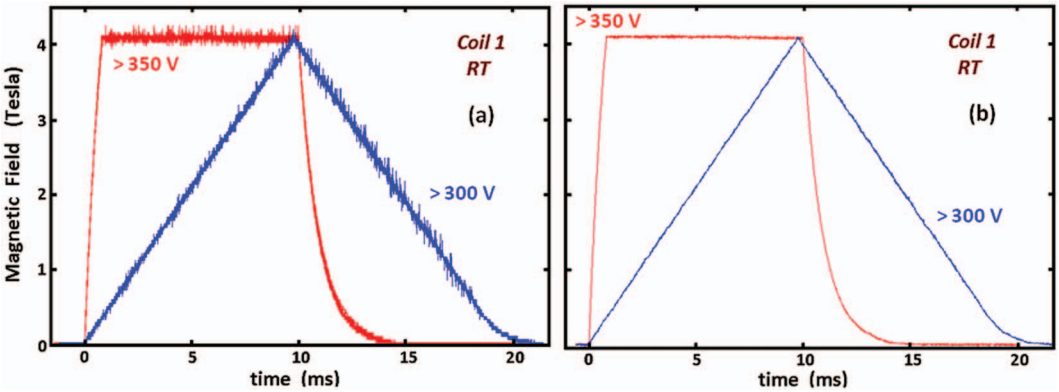

FIG. 5. (a) Ten consecutive 4 tesla flat-tops and 4-tesla-peaked triangular pulses with Coil 1 at room temperature (RT) with a waiting time of ~5–7 min between successive pulses. Numbers beside waveforms denote the individual charging voltages. (b) The two individual averages of the ten pulses shown in (a) – subsequently ruling out the random switching noise and clearly showing the <1% ripple.

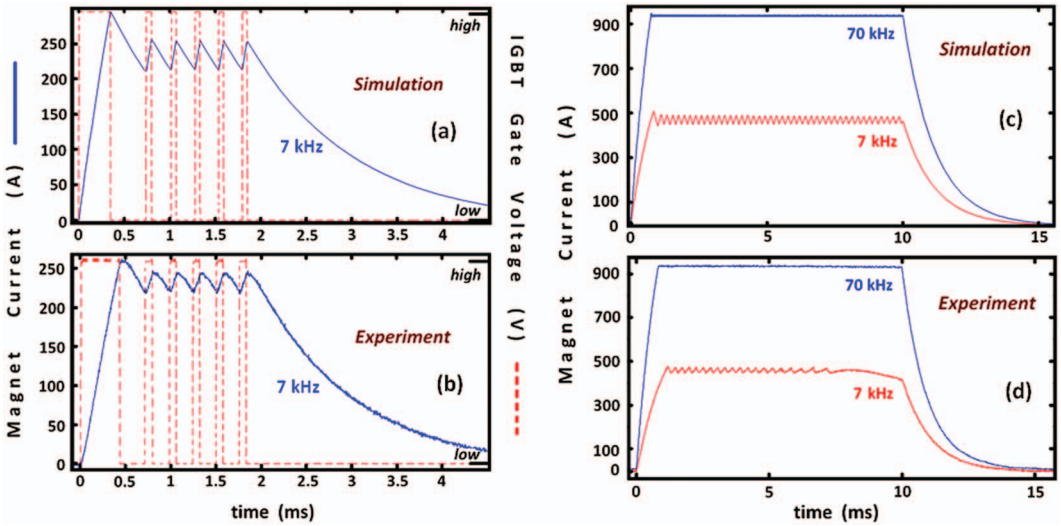

FIG. 6. (a) and (b) Magnet current I (solid lines) and IGBT gate voltage V_{GE} (dashed lines) waveforms for 1 tesla (charging voltage $V_0 = 200$ V); (c) and (d) Two instances of magnet current flat-tops, for 4 tesla ($V_0 = 350$ V) and 2 tesla ($V_0 = 175$ V). All waveforms are with Coil 1 at room temperature. The numbers shown in Hertz represent the f_C of the LPF used in the current transducer output in each case.

can be obtained at the same magnetic fields. Also note that a decrease in ripple would slightly increase the pulse width.

D. Matching experiment with simulation

LT-SPICE was used as the simulation platform. The SPICE models of the IGBT, the Schottky diode, and LM311 are readily available. A model for the IGBT driver SKHI 10/17 was not found and hence we have used the driver chip LTC4440– several of them in parallel. The driver is very important in the simulations since the comparator alone is not sufficient to drive the IGBT gates. SPICE often ceases to simulate especially if spurious inductances are added in the IGBT collector path. To tackle this issue, the current and voltage tolerances in the SPICE settings can be relaxed to lower values, e.g., 1 A and 1 mV. For a high voltage and high current circuit, such resolutions do not significantly affect the results. Simulation waveforms and those experimentally obtained for the magnet current I and the IGBT gate voltage V_{GE} are compared in Fig. 6.

We see that the behavior of our setup can be fairly predicted from the simulations. Apart from checking the magnet current waveforms and the IGBT gate voltages, the transient voltage and current spikes on the IGBTs and the diodes were also compared and were generally found to roughly agree. Note that according to the simulations, with a capacitor charging voltage of 350 V and $f_C \sim 70$ kHz, the total power dissipated by 20 IGBTs during a 10 ms 900 A flat-top pulse is 4 kW and this gives a ripple of <1%. Instead, if $f_C \sim 7$ kHz, simulation shows that the power dissipated drops by 40% to ∼1.6 kW, with a ripple of 10% (experimentally observed to be ∼5%).

IV. CONCLUSION

We present a simple, easy-to-build, table-top CWM, driven by a capacitor bank, capable of producing virtually any user-shaped magnetic field waveform up to 10 tesla. Controlled waveforms can be reproducibly produced up to 4 tesla at room temperature, and up to 10 tesla at liquid nitrogen temperature with our setup. Maximum field (B), maximum slope of the field (dB/dt), and maximum pulse width achievable from the table-top CWM are limited by the magnet coil and the input energy (capacitor bank and its charging voltage).

We also conjecture that our setup can be scaled up (by paralleling more IGBTs and Schottky diodes, and by increasing the input energy) to higher magnetic fields. At present, the maximum current handled by the IGBT and diode modules is 1 kA. We have successfully switched currents double this value – whose results we do not present here.

Also, the same setup may be operated in semi-continuous mode (for a few seconds) by using a capacitor bank or a different power supply – following the works done in Refs. 24 or 23, respectively – as long as the IGBT power dissipation and the magnet coil heating is kept under control.

ACKNOWLEDGMENTS

We are thankful to Dr. Bhavtosh Bansal and Dr. OVSN Murthy for setting up the first pulsed magnets in the lab that served as a foundation to this project. Mr. Jagadheeshan of Manju Electronics, Bangalore, and Mr. Ravi Chawla of Universal Electronics, Bangalore, deserve special mention for making the PCBs and the IGBTs readily available.

[1] *High Magnetic Fields Science & Technology Vol–1*, edited by F. Herlach and N. Miura (World Scientific, Singapore, 2003).
[2] D. B. Montgomery, *Solenoid Magnet Design* (Wiley-Interscience, New York, 1969), pp. 1–10 and 190–225.
[3] R. Gersdorf, P. H. Frings, J. J. M. Franse, and F. R. de Boer, Physica B **201**, 530 (1994).
[4] L. J. Campbell, H. J. Boenig, D. G. Rickel, J. B. Schillig, H. J. Schneider-Muntau, and J. R. Sims, Physica B **216**, 218 (1996).
[5] R. Grossinger, H. Sassik, R. Hauser, E. Wagner, K. Reiterer, P. Rzetecki, and M. Taraba, Physica B **294**, 555 (2001).

[6]R. Gersdorf, F. A. Muller, and L. W. Roeland, Rev. Sci. Instrum. **36**, 1100 (1965).
[7]M. Jaime, R. Movshovich, J. L. Sarrao, J. Kim, G. Stewart, W. P. Beyermann, and P. C. Canfield, in The Proceedings of the Physical Phenomena at High Magnetic Fields - III, Tallahassee, Florida, 1998.
[8]D. R. Khokhlov, I. I. Ivanchik, A. de Visser, and A. V. Nikorich, Semicond. Sci. Technol. **8**, S352 (1993).
[9]K. Kamigaki, A. Hoshi, M. Fuse, M. Ohashi, and T. Kaneko, J. Magn. Magn. Mater. **11**, 328 (1979).
[10]R. Verhoef, R. J. Radwanski, and J. J. M. Franse, J. Magn. Magn. Mater. **89**, 176 (1990).
[11]R. Verhoef, F. R. de Boer, J. J. M. Franse, C. J. M. Denissen, T. H. Jacobs, and K. H. J. Buschow, J. Magn. Magn. Mater. **80**, 41 (1989).
[12]P. Svoboda, P. Javorsky, M. Divis, V. Sechovsky, K. Prokes, F. R. de Boer, A. V. Andreev, M. I. Bartashevich, M. Torikachvili, H. Nakotte, A. Lacerda, H. Sugawara, and Y. Onuki, Physica B **211**, 172 (1995).
[13]J. J. M. Franse, F. R. de Boer, P. H. Frings, and A. de Visser, Physica B **201**, 217 (1994).
[14]G. S. Boebinger, A. H. Lacerda, H. J. Schneider-Muntau, and N. Sullivan, Physica B **294**, 512 (2001).
[15]L. J. M. van de Klundert, H. P. van de Braak, and E. A. Gijsbertse, Physica B **90**, 237 (1977).
[16]L. J. M. van de Klundert, E. A. Gijsbertse, and H. P. van de Braak, Physica B **94**, 41 (1978).
[17]A. Gerber, J. N. Li, Z. Tarnawski, J. J. M. Franse, and A. A. Menovsky, Phys. Rev. B **47**, 6047 (1993).
[18]T. Ida, M. Watasaki, Y. Kimura, M. Miki, and M. Izumi, J. Phys.: Conf. Ser. **234**, 032023 (2010).
[19]T. Ida, H. Matsuzaki, E. Morita, H. Sakashita, T. Harada, H. Ogata, Y. Kimura, M. Miki, M. Kitano, and M. Izumi, J. Phys.: Conf. Ser. **43**, 539 (2006).
[20]V. V. Nesterov and A. R. Donaldson, in *The Proceedings of the Particle Accelerator Conference*, Dallas, Texas, 1995, Vol. 2, pp. 1251–1253.
[21]L. Bartelson and J. Walton, IEEE Trans. Nucl. Sci. **NS-32**, 3755 (1985).
[22]*Pulse Generators*, edited by G. N. Glasoe and J. V. Lebacqz (McGraw-Hill, New York, 1948), pp. 175–224.
[23]D. M. Sousa, P. A. L. Fernandes, G. D. Marques, A. C. Ribeiro, and P. J. Sebastiao, Solid State Nucl. Magn. Reson. **25**, 160 (2004).
[24]D. M. Grishin, V. P. Gubanov, A. V. Gunin, S. D. Korovin, and A. S. Stepchenko, in *The Digest of Technical Papers, Pulsed Power Plasma Science*, Las Vegas, 2001, Vol. 2, pp. 1638–1641.
[25]J. Wang, T. Fors, and G. Sprau, in *The Proceedings of the 8th European Particle Accelerator Conference*, Paris, 2002, pp. 2508–2510.
[26]V. K. Khanna, *IGBT Theory & Design* (IEEE/Wiley-Intercience, New York, 2003).
[27]M. T. Rahimo and N. Y. A. Shammas, IEEE Trans. Ind. Appl. **37**, 661 (2001).
[28]M. Trivedi and K. Shenai, IEEE Trans. Electron Devices **45**, 2537 (1998).
[29]Y. Zhang, S. Sobhani, and R. Chokhawala, in *The Proceedings of the 1st International Conference on Power Electronics and Motion Control*, Beijing, 1994, pp. 261–269.
[30]S. J. Finney, B. W. Williams, and T. C. Green, IEEE Trans. Ind. Appl. **32**, 155 (1996).
[31]International Rectifiier Application Notes, AN 990, www.irf.com/technical-info/appnotes/an-990.pdf.
[32]J. C. Joyce, Ph.D. dissertation, University of Cambridge, May 2001.